Zeeman Anisotropy Fluorescence Spectroscopy, Characteristic Radiative Lifetimes, and Novel Site Symmetries in KCl:Sm^{2+}†

F. K. Fong, M. N. Sundberg, R. H. Heist, and C. R. Chilver
Department of Chemistry, Purdue University, Lafayette, Indiana 47907
(Received 6 July 1970)

By means of Zeeman anisotropy fluorescence (ZAF) and its field dependence (up to 55.8 kG), the authors have investigated the 4.2 K narrow-line fluorescence of KCl: Sm^{2+} and identified some hitherto unreported Sm^{2+} sites. The strong no-field line at 7693.5 Å ($^5D_0 \rightarrow {}^7F_3$) and a very weak no-field line at 8742.8 Å ($^5D_0 \rightarrow {}^7F_5$) are shown to be of C_{3v} symmetry origin. The 24.5-kG ZAF pattern observed in the 7696–7700-Å ($^5D_0 \rightarrow {}^7F_3$) region has been identified to originate from a type-II C_s site. The 26.5-kG ZAF patterns of the C_{3v} no-field line at 7693.5 Å and the type-I C_s no-field line at 7694.5 Å overlap in the 7693–7695.3-Å region, and are elucidated through the field dependence of their Zeeman components. Characteristic radiative lifetimes of the $^5D_0$ level in several Sm^{2+} symmetry types have been determined from dominant transitions to the ^7F_J ($J \leq 4$) levels. There are two distinct C_{4v} sites: one with a lifetime of 9.5 msec, and the other 11.2 msec. C_{2v} and type-I C_s sites have lifetimes of 10.5 and 10.8 msec, respectively, which are indistinguishable within the experimental error. The role of O^{2-} compensation of Sm^{2+} in addition to K^+ vacancy compensation in KCl is discussed in terms of these findings.

I. INTRODUCTION

The law of equilibrium distribution which governs the low-temperature pair formation of divalent cations and cation vacancies in alkali halides[1] and that of trivalent cations and interstitial anions in alkaline-earth halides[2] has been useful in the interpretation and prediction of spectroscopic data on compensated lattices[2–7] in which aliovalent cations and lattice defects interact as ions of opposite unit charges in a crystalline solution. Idealized calculations[1] for KCl: Sm^{2+} ions show that at $T \sim 500$ K, all the Sm^{2+} ions are paired with K^+ vacancies. The dominant pairs, in the order of their relative importance, are the $C_{4v}(2, 0, 0)$, $C_s(2, 1, 1)$, $C_{2v}(1, 1, 0)$, $C_1(3, 2, 1)$, $C_s(3, 1, 0)$, $C_{2v}(2, 2, 0)$, and $C_{3v}(2, 2, 2)$ Sm^{2+}-K^+ vacancy pairs [where the notations C_{4v}, C_s, C_{2v}, and C_1 denote the site symmetry of the Sm^{2+} ion, and the integers in parentheses, e.g., (2, 0, 0), give the lattice position of the vacancy with the divalent cation at the origin], of which the first three account for approximately 90% of the Sm^{2+} ions. The problem of site distribution is often complicated by possible oxygen contamination, in which case the Sm^{2+} ion sees a second site symmetry distribution due to Sm^{2+}-O^{2-} pair formation.[6,7]

There are fourteen dominant (4.2 K narrow-line fluorescence) transitions in KCl: Sm^{2+} spanning the wavelength region 6891–9440 Å.[3] These lines approximately follow the Landé interval rule, and probably arise from the radiative decay of the $^5D_0$ to the ^7F_J levels of the $4f^6$ ground configuration in Sm^{2+}.[6] All these fourteen lines, as well as weaker fluorescence lines of KCl: Sm^{2+}, show Zeeman effects under external magnetic fields up to 93.5 kG.[3–7] Through Zeeman anisotropy fluorescence (ZAF) determinations, the no-field lines[7] at 7014.7 Å (0 → 1) and 7264.4 Å (0 → 2) have been attributed to C_{2v} symmetry origin, the no-field lines at 7282.8 Å (0 → 2),[7] 7304.6 Å (0 → 2),[7] 8204.9 Å (0 → 4),[3] and 9439.1 and 9440.0 Å (0 → 6)[3] have been attributed to C_{4v} symmetry origin, and the no-field lines at 7031.7 Å (0 → 1),[7] 7694.5 Å (0 → 3),[5] and 8778.4 Å (0 → 5)[5] have been attributed to C_s site symmetry origin. The 0 → 0 line at 6891.9 Å as well as the diffuse no-field lines at 7048.2 Å (0 → 1) and 7327.6 Å (0 → 2) show Zeeman shifts at high fields, but they do not give rise to discernible ZAF patterns even at 93.5 kG.[7] The sites responsible for these lines thus far remain unknown. The assignment[5] of the no-field line at 7694.5 Å to the $C_s(2, 1, 1)$ pattern is tentative due to the presence of the no-field line at 7693.5 Å (the symmetry origin of which has yet to be determined) in its close proximity: Additional work is necessary to isolate the overlapping ZAF patterns, which at 26.5 kG occur in the 7693–7695.3-Å region.

There are three main goals in the present work: (i) to determine the site symmetry origin of the thus far unknown no-field line at 7693.5 Å (0 → 3) which, in turn, will enable us to confirm the $C_s(2, 1, 1)$ origin of the no-field line at 7694.5 Å; (ii) to examine the possible existence of site symmetries other than C_{4v}, C_{2v}, and $C_s(2, 1, 1)$; and (iii) to propose radiative lifetime measurements as a new technique for the site symmetry determination of lines which do not give rise to discernible ZAF patterns.

In achieving goal (i), we have resorted to field dependence investigations in which ZAF patterns are traced to their original no-field lines. The angular dependence of the Zeeman components in a ZAF pattern is ascertained through their line intensities

as recorded with tracings of the photographic plates from a high-resolution comparator microdensitometer. In accomplishing goal (ii), we have examined the schematic ZAF patterns for all the possible Sm^{2+} sites in KCl. A systematic search has been made among the weaker lines in all the J manifolds for novel site symmetries [C_{3v}, C_s(II), and C_1] which have not been previously observed. Goal (iii) is achieved by establishing the fact that for a given site there is one and only one characteristic radiative decay lifetime from a single excited level. As a result of these investigations, we wish to report (i) the discovery of the C_{3v} symmetry origins of the no-field line at 7693.5 Å(0 → 3) and a very weak no-field line at 8742.8 Å(0 → 5); (ii) the observation of a type-II C_s ZAF pattern in the 7696–7700-Å region (0 → 3) which is probably of C_s(3, 1, 0) origin; and (iii) the observation of two different dominant C_{4v} sites as well as the probable C_{2v} assignment of the 6891.9-Å(0 → 0) line by means of characteristic lifetimes. The complications of the site symmetry distribution by the presence of O^{2-} compensation emerge as a result of this investigation, which will be discussed in some detail.

II. THEORETICAL FRAMEWORK

A. ZAF Patterns of Allowed Sm^{2+} Site Symmetries

In the free-ion state, the LS coupling scheme is usually considered as a good approximation for the Sm^{2+} ion. The $|f^6\alpha LSJM)$ free-ion states, where α denotes all other quantum numbers not specified, are employed as the zeroth-order wave functions in our problem. In a crystalline lattice, the crystal field potential contributes a term to the total Hamiltonian of the Sm^{2+} ion. The term is usually expanded as a series of spherical harmonics,

$$H_{cf} = \sum_{l,m,i} A_l^m r_i^l Y_l^m(\theta_i, \phi_i) , \qquad (1)$$

where the expansion coefficients A_l^m are determined by the position of the charge compensation in a complex of a given site symmetry. In terms of the Wigner-Eckart theorem, a typical matrix element of the crystal field perturbation matrix can be written[8]

$$(f^6\alpha LSJM|\mathcal{H}_{cf}|f^6\alpha SLJM') = B_l^m C^{J\,l\,J}_{M\,m\,M'}(\alpha SLJ||Y_l||\alpha SLJ) ,$$

$$B_l^m = \langle r^l\rangle A_l^m , \qquad (2)$$

where $C^{J\,l\,J}_{M\,m\,M'}$ is a Wigner coefficient and $(\alpha SLJ||Y_l||\alpha SLJ)$ a reduced matrix element. The diagonalization of the crystal field perturbation matrix results in the crystal field states, provided that coefficients B_l^m are known.

If one assumes the point charge model, the crystal field expansion coefficients A_l^m are

$$A_l^m = (4\pi/2l+1)\textstyle\sum_j (q_j e^2/R_j^l + 1) Y_l^{m*}(\theta_j, \phi_j) , \qquad (3)$$

where R_j is the distance between the jth ion and the central ion, the sum extends over all the ions of the lattice, and q_j is the effective charge of the jth ion. The point charge model, however, ignores effects arising from charge overlap, covalency, polarization of the lattice about the central ion, as well as the lattice distortion about the divalent cation-compensation pair. Equation (3) is thus often invalid, and the coefficients B_l^m are best treated as experimental parameters. When only one site symmetry exists or is assumed for the rare-earth ion, it is possible to identify the representation origin of a given transition through conventional spectroscopic techniques such as polarization and group theoretical selection rules, and diagonalization of the $\mathcal{H}_{cf}$ matrix can be readily achieved by parameter fitting of the B_l^m coefficients.

In compensated lattices such as KCl : Sm^{2+} in which the fluorescence is made up of a superposition of Sm^{2+} fluorescence lines arising from various sites, the above procedure is not possible unless the site origin of each line is determined. The polarized excitation technique employed by Bron and Heller[9] in the determination of dipole origin, representation origin, and site origin is unique only for the 0 → 0 transition. For all the other transitions, it is necessary to assume the site origin or the polarization of the excitation, which is not justified in KCl : Sm^{2+}. One unique method for the determination of symmetry origin is the ZAF technique in which characteristic patterns of the angular dependence of energy shifts of the Zeeman components are readily recognizable for each of the site symmetries allowed for the Sm^{2+} ion due to geometric restrictions of the fcc KCl lattice.

Under an external magnetic field, an additional term must be added to the total Hamiltonian of the central Sm^{2+} ion in the form

$$\mathcal{H}_m = g_\lambda \mu_B H_0[\cos\theta_H J_Z + \tfrac{1}{2}\sin\theta_H (e^{i\phi_H} J_- + e^{-i\phi_H} J_+)] , \quad (4)$$

where μ_B is the Bohr magneton, g_λ the Landé g factor, H_0 the effective magnetic field strength, θ_H the angle between the $\vec{H}$ field and the Z axis, and ϕ_H the corresponding azimuthal angle. In axial symmetries such as C_{2v}, C_{3v}, and C_{4v}, Z is taken to be the rotational C axis. In C_s symmetries Z is taken to be the axis $\perp$ to the reflection (XY) plane. In KCl : Sm^{2+} there are, in all, six types of site symmetries in K^+ vacancy compensation: C_{2v}, C_{3v}, C_{4v}, C_s(I), C_s(II), and C_1 which are typified by the C_{2v}(1, 1, 0), C_{3v}(2, 2, 2), C_{4v}(2, 0, 0), C_s(2, 1, 1), C_s(3, 1, 0), and C_1(3, 2, 1) Sm^{2+}-K^+ vacancy pairs, respectively. The ZAF patterns for C_{2v}, C_{4v}, and C_s(I) have been described previously.[3,5] Here, we shall consider the theoretical patterns of the C_{3v} and C_s(II) sites, which are shown in Fig. 1 along with the schematic ZAF patterns for C_{2v}, C_{4v}, C_s(I), and C_1 sites. No detailed discussion for the C_1 ZAF pattern will be

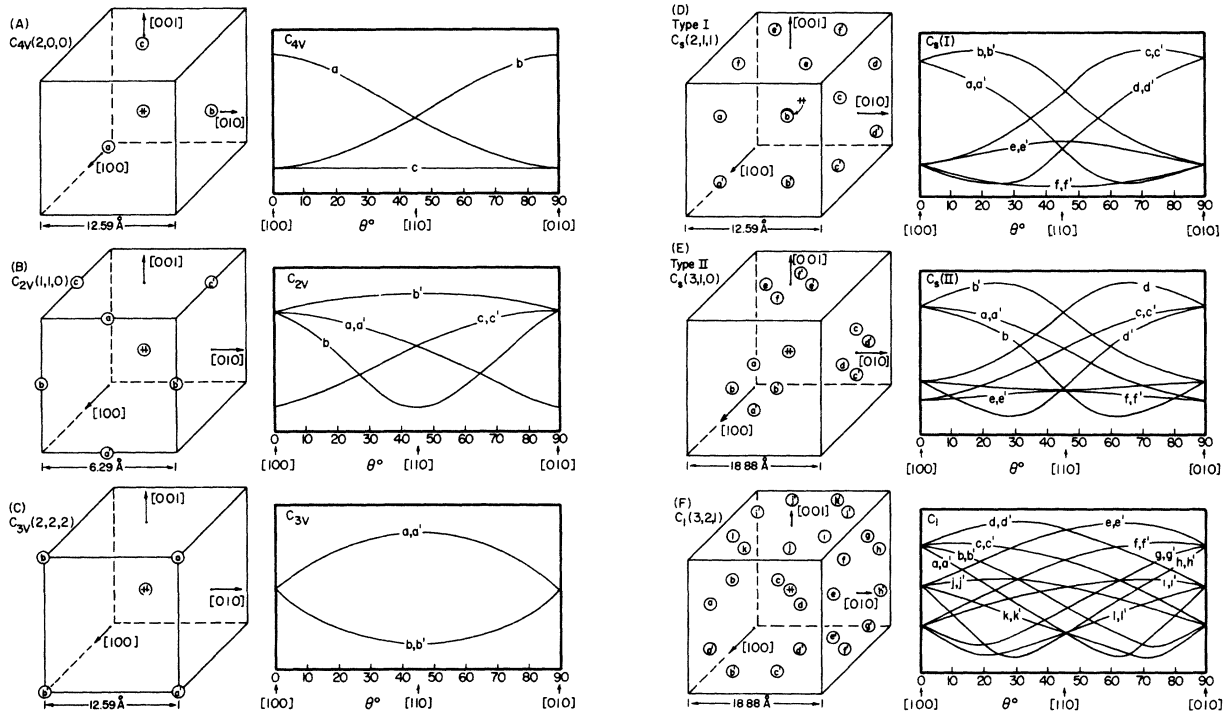

FIG. 1. Equivalent magnetically distinguishable vacancy sites and corresponding schematic ZAF patterns [with $\vec{H}$ rotating in (001) plane] for the six typical Sm^{2+} site symmetries allowed for K^+ vacancy compensation as exemplified by (a) three equivalent $C_{4v}(2, 0, 0)$ sites, (b) six equivalent $C_{2v}(1, 1, 0)$ sites, (c) four equivalent $C_{3v}(2, 2, 2)$ sites, (d) twelve equivalent type-I $C_s(2, 1, 1)$ sites, (e) twelve equivalent type-II C_s (3, 1, 0) sites, and (f) 24 equivalent $C_1(3, 2, 1)$ sites. The ZAF patterns are deduced on the basis of a transition between two nondegenerate levels.

given in the text since it has not been observed in the present investigation or elsewhere.

For $C_{3v}(2, 2, 2)$ Sm^{2+}-K^+ vacancy pairs there are eight equivalent sites, four of which are shown in Fig. 1(c) at the corners of a face of a cube whose center is occupied by the Sm^{2+} ion. Each side of the cube measures $4a$, where $a = 3.15$ Å is the K^+-Cl^- distance of separation. Since the magnetic field is invariant upon inversion, the $[lmn]$ and $[\bar{l}\bar{m}\bar{n}]$ crystal axes are equivalent, and the four remaining sites are indistinguishable from the four sites shown through an inversion of coordinates. With $\vec{H} \parallel [100]$, all the sites are equivalent, and only one line will arise from them. As $\vec{H}$ is rotated towards [010] in the (001) plane, two lines arise due to the two sets of equivalent sites: (i) a, a'; (ii) b, b'. These two lines will reach a maximum separation when $\vec{H}$ is in the [110] direction and will merge back together with $\vec{H}$ in the [010] direction. [See anisotropy pattern in Fig. 1(c).]

For the type-II $C_s(3, 1, 0)$ site there are 24 equivalent sites. In Fig. 1(e), twelve of these sites are shown lying on three faces of a cube of $(6a)^3$. Each site lies $+a$ or $-a$ away from the center of a cube face in one of the six major crystal planes $\{100\}$. Again, the remaining twelve sites are obtained through a coordinate inversion. With $\vec{H}$ in the [100] direction there are three sets of equivalent sites: (i) a, a', b, b'; (ii) d, d', f, f'; and (iii) c, c', e, e' which give rise to three lines. As $\vec{H}$ is rotated towards [010] in the (001) plane, there is splitting of the above three lines into eight lines corresponding to the eight sets of equivalent sites: (i) b'; (ii) a, a'; (iii) b; (iv) d; (v) f, f'; (vi) d'; (vii) c, c'; and (viii) e, e'. When $\vec{H} \parallel [110]$, the pattern will merge into three lines according to the groups (i) b', d; (ii) a, a', c, c'; and (iii) b, d', e, e', f, f'. As $\vec{H}$ rotates away from [110], eight lines appear due to the same eight sets of equivalent sites as previously mentioned. Finally, when $\vec{H}$ reaches [010], the eight lines merge into three corresponding to the following sets of equivalent sites: (i) c, c', d, d'; (ii) b, b', e, e'; and (iii) a, a', f, f'.

It is important to realize that it is possible to identify experimental ZAF patterns according to the schematic patterns shown in Fig. 1 without ever having to solve the matrix equations involving the perturbation Hamiltonians of Eqs. (1) and (4). When the no-field line is intense and its Zeeman components well resolved, it is possible to determine its symmetry origin beyond any doubt. Difficulties arise when the ZAF patterns of two no-field lines

of comparable intensities overlap, particularly when a lower-symmetry (and thus more complicated) pattern is involved. Such difficulties are encountered in the case of the overlapping ZAF patterns of the 7693.5- and 7694.5-Å no-field lines in $0 \rightarrow 3$. Although the $C_s(2, 1, 1)$ origin of one of the two lines was apparent,[5] an additional anisotropic Zeeman component was not satisfactorily accounted for. In a detailed analysis given in Sec. IV, we shall overcome these difficulties in arriving at the correct solution.

B. Characteristic Radiative Lifetimes

Lifetime measurements on rare-earth ions in ionic crystals have been reported by a number of authors in recent years.[10–13] Usually, these works focused on the temperature dependence or concentration dependence of the lifetimes. In the present work, we shall discuss the use of lifetime measurements as a tool for distinguishing the various symmetry types of Sm^{2+} in KCl.

Fluorescence of KCl: Sm^{2+} is observed upon optical pumping of the $4f^5d$ bands, which lie at about 15 500 cm^{-1} above the $^7F_0$ level. All the fluorescence lines arise from radiative decay from the ^5D multiplet to the ^7F multiplet. In general, the effective decay time for a group of n excited levels in a given site is given by

$$\frac{1}{\tau_{eff}} = \sum_{i=1}^{n} g_i A_i \exp\left(\frac{E_1 - E_i}{kT}\right) \Big/ \sum_{i=1}^{n} g_i \exp\left(\frac{E_1 - E_i}{kT}\right), \tag{5}$$

where A_i is the total Einstein spontaneous-emission probability from the ith level to all lower levels, and g_i is the degeneracy of the ith level. Here, we have assumed that a Maxwell-Boltzmann distribution of the n excited levels is achieved through rapid phonon processes and that there are no nonradiative transitions to the ground levels. In KCl: Sm^{2+} all the radiative decay processes probably initiate from the $^5D_0$ level at 4.2 K,[9] and Eq. (1) simplifies to

$$1/\tau_{eff} = \sum_J A(0, J) = 64\pi^4(3h)^{-1} \sum_J \nu_{0J}^3 S(0, J), \tag{6}$$

where 0 and J are the symmetrized crystal states of $^5D_0$ and ^7F_J levels in Sm^{2+}, respectively, ν_{0J} is the frequency of the transition $0 \rightarrow J$, and

$$S(0, J) = \sum |\langle \alpha | \vec{V} | \beta \rangle|^2$$

gives the line strength between the two states 0 and J. Here, α and β are the components of the symmetrized crystal states 0 and J, respectively, and $\vec{V}$ is usually either the magnetic ($\vec{M}$) or the electric ($\vec{P}$) dipole moment operator given by

$$\vec{M} = -e(2mc)^{-1} \sum_i (\vec{L}_i + 2\vec{S}_i)$$

and

$$\vec{P} = -e \sum_i \vec{r}_i,$$

where e is the electronic charge of the electron and m is the mass of the electron. For electric dipole transition moments, only opposite parity components of 0 and J give rise to nonvanishing contributions, while magnetic dipole transition moments arise from matrix elements connecting free-ion states within the $4f^6$ ground configuration. Since 0 and J are unique for a given Sm^{2+} site according to $\mathcal{H}_{cf}$ in Eq. (1), it follows that each type of Sm^{2+} site must possess a distinct *and characteristic* effective radiative decay lifetime. The important experimental handle on the problem of site distribution which emerges from the above argument is that if a given Sm^{2+} ion site radiatively decays through several fluorescence transitions, its effective decay time can be determined by monitoring any one of these fluorescence transitions. Conversely, if the characteristic radiative decay lifetimes of the various Sm^{2+} symmetry species are known, it is in principle feasible to determine the symmetry origin of any fluorescence transition by measuring its effective decay time and matching it with one of the known characteristic lifetimes. In general, even if the decay process is not purely radiative, and $1/\tau_{eff}$ is the sum of *all* the decay probabilities, radiative and otherwise, the lifetime is still characteristic of the site symmetry. These ideas will be further developed in the following sections as we describe the lifetime measurements and their interpretations.

III. EXPERIMENTAL PROCEDURE

KCl: Sm^{2+} crystal samples were grown in a H_2 atmosphere using the Czochralski technique.[14] An EDTA analysis was carried out to show that the crystals contained 3.6×10^{18} (Sm^{2+} ions) cm^{-3}. All spectra were measured spectrographically at 4.2 K. A 600-W tungsten-halogen lamp was used to pump in the 3800–6000-Å broad bands. The crystal sample was suspended in a narrow Dewar tip and submerged in liquid He. For low magnetic fields (up to 26.5 kG) a Varian V-3900 12-in. low-impedance electromagnet with a $1\frac{1}{4}$-in. gap was used. The 4.2 K anisotropy and low field dependence spectra were taken on a 2-m Jarrell-Ash (model 75-174) spectrograph with a grating (102 mm × 102 mm, 1180 g/mm) blazed at 1.0 μ. The spectra were recorded on Eastman Kodak N and hypersensitized M plates. Higher field measurements were made at the Francis Bitter National Magnet Laboratory employing a 2-m Bausch and Lomb grating spectrograph. Reading of the photoplates was accomplished by means of a direct scanning Grant-Daytex comparator microdensitometer which was coupled to a Varian Statos I (model 150) electrostatic recorder. The comparator has a reproducibility of ± 0.25 μ and is equipped with both a viewing screen and a split-im-

age oscilloscope display which enhances speed and accuracy of photoplate allignment. A photomultiplier takes transmittance (T) data and presents them as density values ($1 - T$).[15] Reproducibility was in most cases better than 0.05 Å.

In lifetime measurements, the crystal was pumped with the light from an EGG FX-12 flashlamp. The resulting fluorescence at 4.2 K, passed through a 0.25-m Jarrell-Ash grating monochromator, was registered on a photomultiplier tube (RCA 7265) with an S-20 response. The signal was recorded photographically from an oscilloscope trace. A combination of blue and red filters prevents the pump light from entering the monochromator.

IV. EXPERIMENTAL RESULTS AND INTERPRETATIONS

The $\vec{H}\|[100]$ field dependence (up to 55.8 kG) of the Zeeman components from $0 \rightarrow 3$ transitions in the 7690–7702-Å region is shown in Fig. 2. The salient features of Fig. 2 are (i) The strong (s) zero-field 7694.5-Å line splits into two Zeeman components, the shorter wavelength of which crosses over the very strong (vs) line (originating from the 7693.5-Å zero-field line) at 21.6 kG. (ii) The 7693.5-Å line appears to remain as a single component. The very weak (vw) line which appears on its long-wavelength side at fields higher than 30 kG

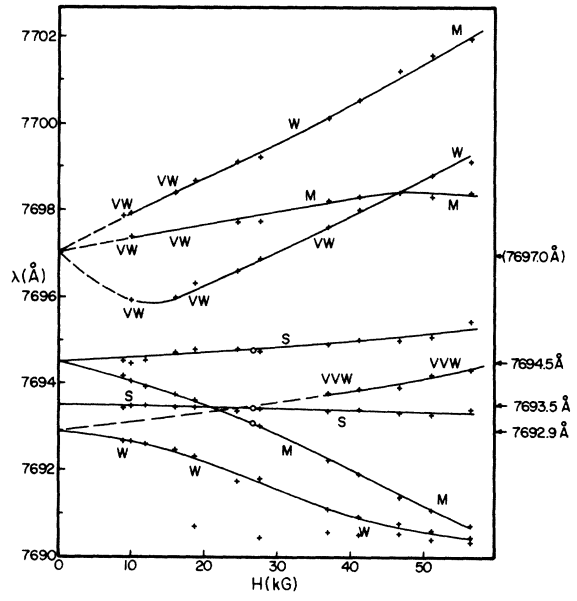

FIG. 2. Field dependence ($\vec{H}\|[100]$) of the Zeeman components of the no-field ($0 \rightarrow 3$) lines at 7692.9, 7693.5, 7694.5, and 7697.0 Å. Intensities are indicated by S = strong, M = medium, W = weak, VW = very weak, and VVW = very very weak. The dashed lines indicate extrapolations to zero field. The open circles indicate that the values correspond to the 0° values of the 26.5-kG ZAF patterns in Fig. 4.

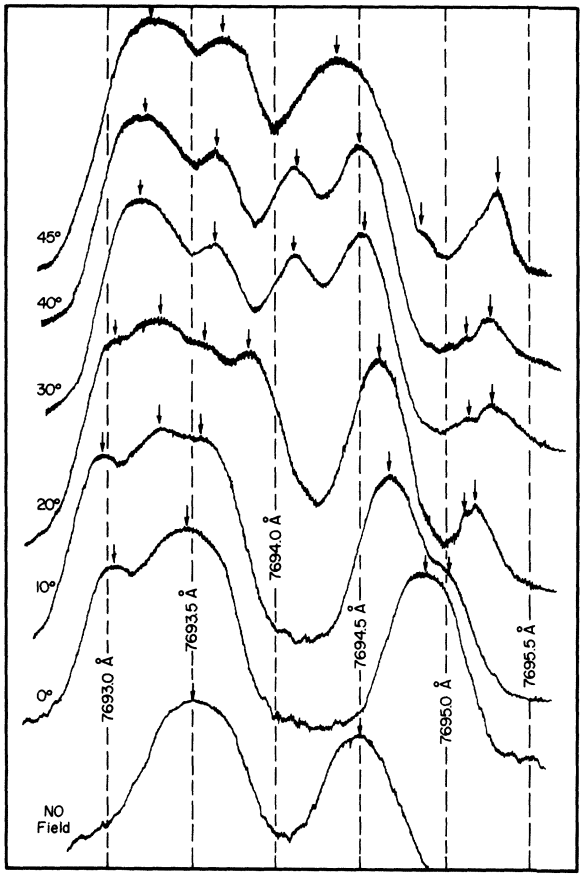

FIG. 3. 4.2 K fluorescence lines in the $7693 \rightarrow 7695.5$-Å region: no-field and $\vec{H}$ (26.5 kG) at 0°, 10°, 20°, 30°, 40°, and 45° from [100] in the (001) plane. Arrows correspond to points plotted in the ZAF patterns of Fig. 4.

most probably originates from the weak no-field at 7692.9 Å. (iii) The lines which appear in the long-wavelength region (> 7695 Å) exhibit notable field dependence in their intensities. Their no-field origin is not observed due to vanishingly low intensities. The field dependence of the Zeeman components makes possible an extrapolation to a single no-field origin at 7697.0 Å.

The anisotropic Zeeman splitting (at $H = 26.5$ kG) behavior of the two strong no-field lines at 7693.5 and 7694.5 Å is shown in Fig. 3. Here $\vec{H}$ is rotated in the (001) plane, and angular dependence of the Zeeman components are shown with $\vec{H}$ 0°, 10°, 20°, 30°, 40°, and 45° away from [100]. The corresponding peak positions of the resolved lines are plotted against the angle of $\vec{H}$ rotation in Fig. 4.

With $\vec{H}\|[100]$ ($H = 26.5$ kG) three Zeeman components are observed at 7693.0_4, 7693.4_6, and 7694.8_8 Å. They are shown as open circles in Fig. 2. It is clear from this comparison that the components

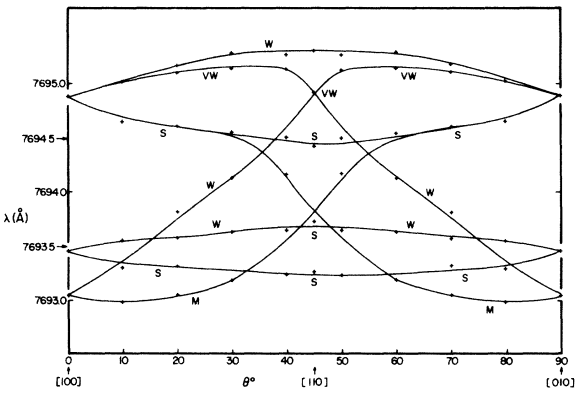

FIG. 4. Overlapping C_s(I) and C_{3v} 26.5-kG ZAF patterns observed for the 0→3 no-field lines (indicated by arrows) at 7694.5 and 7693.5 Å, respectively, with $\vec{H}$ rotated in the (001) plane.

at 7693.0_4 and 7694.8_8 Å belong to the 7694.5-Å no-field line, a crucial piece of information not available to us without the field dependence data given in Fig. 2. The 7693.4_6-Å component (0°) arises from the 7693.5-Å no-field. In view of its lack of splitting with $\vec{H}\|[100]$ (Fig. 2), it is most probably due to a singlet transition of C_{3v} origin. [See ZAF pattern in Fig. 1(c).] Upon angular rotation of the magnetic field, it splits into two subcomponents (Figs. 3 and 4), giving rise to a ZAF pattern that is immediately recognizable as a C_{3v} pattern [Fig. 1(c)]. The 0° component at 7694.8_8 Å splits into three subcomponents as the field angle increases. The 0° component at 7693.0_4 Å must merge into the component at 7694.8_8 Å after 90° rotation of $\vec{H}$ since both of these two components arise from the same no-field origin (Fig. 2). With this information we readily arrive at the experimental ZAF pattern [which agrees perfectly with the C_s(I) schematic pattern shown in Fig. 1(d)] arising from the 7694.5-Å no-field line by simply connecting the points observed in addition to these assigned to the C_{3v} pattern arising from the 7693.5-Å line.

The angular dependence of the Zeeman components (at H = 24.5 kG) in the 7696–7700-Å region (0→3) is shown in Fig. 5(a). These weak Zeeman components arise from a single no-field line which is manifested through extrapolation from field dependence data in Fig. 2. When a single no-field line splits into three components with $\vec{H}\|[100]$, it must be of either C_s(II) or C_1 symmetry origin [see Figs. 1(e) and 1(f)]. Although several weak components are missing, a C_s(II) interpretation of the observed lines gives a reasonable representation of the experimental data. In Fig. 5(b) we present evidence for the observation of a very weak C_{3v} ZAF pattern which arises from the weak no-field line at 8742.8 Å (0→5).

Because of apparatus limitations, lifetime measurements are restricted to dominant lines in 0→J transitions with $J \leq 4$. In addition to the narrow-line 0→J transitions, broad-band transitions are also observed. Typically, the broad-band fluorescence (probably $d \rightarrow f$) lifetimes (~ 10^{-1} msec) were observed to be orders of magnitude shorter than those (~ 10 msec) of the narrow-line fluorescence. The results of lifetime measurements on dominant 0→J lines are given in Table I, along with the corresponding symmetry identifications. The lifetimes have been determined from least-squares fits of exponentials to oscilloscope traces and are given in Table I as averages of three or four trials, along with their standard deviations.

We have found two C_{4v} lifetimes: ~ 9.5 msec at 7282.8 Å (0→2) and 8204.9 Å (0→4); ~ 11.2 msec at 7304.6 Å (0→2). This finding is in agreement with the earlier conclusion[6,7] from ZAF investigations that at least two dominant C_{4v} sites, most probably the C_{4v}(2, 0, 0) Sm^{2+}-K^+ vacancy pair and the C_{4v}(1, 0, 0) Sm^{2+}-O^{2-} pair, are present.

The two lines at 7048 Å (0→1) and 7327.8 Å (0→2) do not give discernible ZAF patterns at magnetic

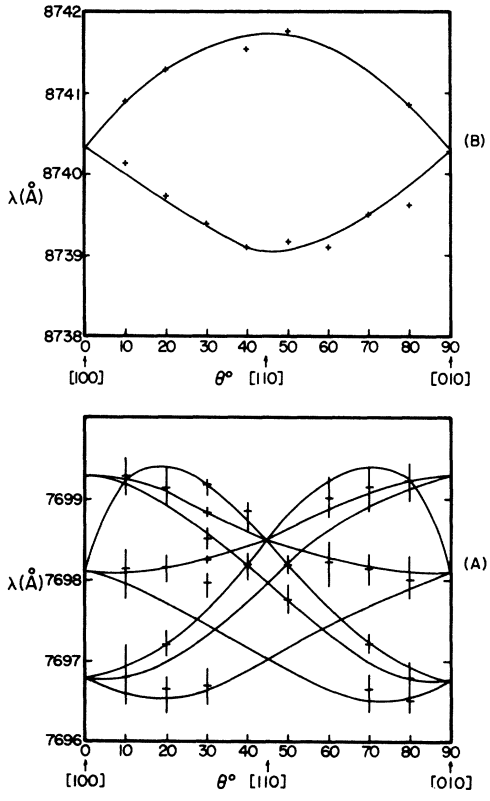

FIG. 5. 4.2 K ZAF patterns with $\vec{H}$ rotated in (001) plane: (a) 24.5-kG C_s(II) ZAF pattern for the weak 0→3 transition in the 7696–7700-Å region; and (b) 26.5-kG C_{3v} ZAF pattern for the weak 0→5 transition in the 8739–8742-Å region.

TABLE I. Symmetry origin determinations of dominant 4.2 K fluorescence lines in KCl : Sm^{2+}.

Transition	λ(Å)	cm^{-1}	Lifetime (msec)	Symmetry	References on symmetry	Comments
0→0	6891.9	14509.8	10.2±0.2	C_{2v}	Present work	0.16-cm^{-1} blue shift at 93.5 kG; no discernible ZAF pattern.
0→1	7014.7	14255.8	10.7±0.2	C_{2v}	7	Resolved ZAF pattern at 93.5 kG.
	7031.7	14221.3	10.8	C_s(?)	7	ZAF pattern observed at 93.5 kG is not well resolved.
	7048.2	14188.0	10.5±0.2	C_{2v} or C_s(I)	Present work	0.08-cm^{-1} red shift at 93.5 kG; no discernible ZAF pattern.
0→2	7264.4	13765.8	10.4±0.4	C_{2v}		Resolved ZAF pattern at 93.5 kG.
	7282.8	13731.0	9.5±0.5	C_{4v}(I)	7, Present work	Good ZAF pattern at 93.5 kG.
	7304.6	13690.0	11.2±0.4	C_{4v}(II)	7, Present work	Resolved C_{4v} ZAF pattern at 93.5 kG with isotropic line due to site c missing [compare with Fig. 1(a)].
	7327.6	13647.0	10.4±0.8	C_{2v} or C_s(I)	Present work	1.22-cm^{-1} red shift; no discernible ZAF pattern.
0→3	7693.5	12988.0	10.3±0.1	C_{3v}	Present work	Resolved overlapping ZAF patterns at 26.5 kG.
	7694.5	12996.3		C_s(I)	5, Present work	
0→4	8204.9	12187.8	9.7±0.8	C_{4v}(I)	3	Resolved C_{4v} ZAF pattern at 26.5 kG with isotropic line due to site c missing.
0→5	8778.4	11391.6		C_s(I)	5	ZAF pattern observed at 26.5 kG is not well resolved.
0→6	9439.1	10594.2		C_{4v}	3	Resolved ZAF patterns at 26.5 kG.
	9440.0	10593.2		C_{4v}		

fields up to 93.5 kG.[7] However, their lifetimes show that they arise from either C_{2v} or C_s sites, which are indistinguishable within the experimental error.

The $J=0$ lines contain a dominant component at 6891.9 Å and a weaker component at 6890.7 Å.[7] Their combined effective decay time is 10.2 msec, which lies on the low side of the lifetime range observed (Table I) for known C_{2v} lines. If we assume the empirical ΔJ odd selection rule[7] for the C_s site (dominant C_s lines are observed only in 0→1, 3, and 5 transitions), the 6891.9-Å (0→0) line is of C_{2v} origin. This assignment is consistent with the polarized excitation experiment by Bron and Heller,[9] which is unique only for the 0→0 transition.

V. DISCUSSION

By means of detailed ZAF analyses and lifetime measurements, we have brought the study of 4.2 K KCl: Sm^{2+} fluorescence to a reasonable state of completion. In an initial paper[3] on ZAF spectroscopic investigation into KCl: Sm^{2+}, the dominant transitions in 0→6 and 0→4 were found to be of C_{4v} symmetry origin, which raised serious doubts to the single $C_{2v}(1, 0, 0)$ complex spectroscopic analysis made by Bron and Heller[9] for the same system. A statistical mechanical calculation[1] was subsequently made for an idealized system of divalent cations charge compensated by K^+ vacancies. It was predicted[1] that a distribution of site symmetries must exist and that the third-nearest-neighbor C_s (2, 1, 1) site is of great prominence in this distribution, which was confirmed[5] by experimental ZAF observations. Of the fourteen dominant fluorescence transitions, ten have been shown in these previous papers[3–7] to arise from C_{4v}, C_s(I), and C_{2v} sites. The symmetry origins of the remaining four lines have been determined in the present work. Results of the various symmetry determinations are tabulated in Table I.

The problem of overlapping ZAF patterns such as those arising from the 7693.5- and 7694.5-Å lines has been dealt with in the preceding paragraphs. There exists still another difficulty which complicates the problem of line symmetry assignment: missing lines in an otherwise well-resolved ZAF pattern. For example, if the isotropic line due to site c [Fig. 1(a)] is missing from the C_{4v} ZAF pattern, the resulting pattern becomes indistinguishable from a C_{2v} pattern with the latter pattern's lines due to sites b and b' [Fig. 1(b)] missing. A C_s(I) pattern [Fig. 1(d)] with the lines due to sites b, b', c, and c' missing could be mistaken for a somewhat distorted C_{2v} pattern. A C_{2v} pattern with the lines due to sites a, a', c, and c' missing gives the appearance of a distorted C_{3v} pattern. These complications are exemplified by the C_{4v} ZAF pattern of the dominant line at 8204.9 Å ($0 \rightarrow 4$) in which the isotropic line is not observed. Its C_{4v} symmetry assignment now appears correct in view of the observed lifetime (9.7 ± 0.8 msec) associated with it, which is in good agreement with the lifetime (9.5 ± 0.5 msec) associated with the 7282.8-Å ($0 \rightarrow 2$) line for which a definitive C_{4v} ZAF pattern was observed at 93.5 kG. The C_{4v} pattern of the line at 7304.6 Å also has its isotropic line missing. Its C_{4v} assignment is again ascertained by the lifetime measurement; the associated characteristic lifetime is 11.2 ± 0.4 msec which lies outside the range of lifetimes given for all the C_{2v} lines (see Table I). The possible observation of a dominant C_{2v} line due to a second C_{2v} site other than $C_{2v} \times (1, 1, 0)$ vacancy pair is very unlikely due to the fact that the probability of finding the $C_{2v}(2, 2, 0)$ vacancy pair is negligibly small[1] and that O^{2-} ion compensation does not give rise to C_{2v} sites.

The observation of two dominant tetragonal sites by lifetimes, C_{4v}(I) with $\tau_{eff} \sim 9.5$ msec and C_{4v}(II) with $\tau_{eff} \sim 11.2$ msec, gives strong support to the earlier conclusion that O^{2-} compensation of Sm^{2+} must be present in KCl: Sm^{2+} giving rise to a second site distribution with the O^{2-} ion (associated with the divalent cation) occupying various possible inequivalent lattice points in the Cl^- sublattice. The role of O^{2-} in charge compensation is further manifested in the observation of the dominant C_{3v} line at 7693.5 Å. According to the statistical calculation,[1] the sixth-nearest-neighbor $C_{3v}(2, 2, 2)$ vacancy pair is quite improbable at ordinary room temperatures from which the samples are quenched to cryogenic temperatures for spectroscopic measurements. The observation of a very weak C_{3v} ZAF pattern such as the one shown in Fig. 5(b) might be attributed to the $C_{3v}(2, 2, 2)$ site. The observation of the C_{3v} line at 7693.5 Å, the most dominant line in $0 \rightarrow 3$, however, can only be interpreted in terms of the observation of the $C_{3v}(1, 1, 1)$ Sm^{2+}-O^{2-} pair, which corresponds to the second-nearest-neighbor pair in the O^{2-} compensation site distribution.

Although the earlier C_s(I) assignment[5] of the no-field line at 7694.5 Å is confirmed in the present paper, the C_s(I) ZAF pattern given in Fig. 4 differs in one important detail from that given[5] in the earlier paper: The 0° Zeeman component at 7693.0_4 Å [Figs. (3) and (4)] was previously attributed[5] to the no-field line at 7693.5 Å while that at 7693.4_6 Å was thought to belong to the C_s pattern. In Sec. IV of the present paper, we have conclusively shown (Figs. 2–4) that such is not the case. We have thus demonstrated the importance of the field dependence data (Fig. 2) in tracing the origin of a ZAF pattern, particularly when overlapping patterns are involved.

The positive confirmation of the C_s(I) pattern is of importance, since the prominent presence of the $C_s(2, 1, 1)$ Sm^{2+}-K^+ vacancy pair represents a crucial feature of the vacancy pair distribution theory.[1,5] If the weak C_s(II) and C_{3v} patterns shown in Fig. 5 correspond to the observations of the fifth and sixth nearest neighbors $C_s(3, 1, 0)$ and $C_{3v}(2, 2, 2)$ Sm^{2+}-K^+ vacancy pairs, respectively, the ZAF technique is apparently capable of detecting the perturbing influences of the vacancy on the Sm^{2+} ion even when the Sm^{2+} vacancy-separation distance is as large as ~ 10 Å. It is interesting to note that in the electron spin resonance studies on (alkali halide): Mn^{2+} systems,[16] Mn^{2+} vacancy pairs beyond the second nearest neighbors were collectively observed as "cubic" sites.

In conclusion, we have definitively shown by means of several spectroscopic methods (ZAF, field dependence, and characteristic lifetime measurements) that a distribution of Sm^{2+} sites exists in KCl. We have further shown that in addition to K^+ vacancies, apparently O^{2-} ions participate in the charge compensation of the Sm^{2+} ions. The method outlined[1] for the divalent cation-vacancy pair distribution can be readily extended to include the presence of O^{2-} ions in the Cl^- sublattice. The problem of compensated lattices is thus well defined within the scope of our investigations.

ACKNOWLEDGMENTS

We wish to acknowledge the generous help of the management of Francis Bitter Magnet Laboratory where the high-field spectrographic plates were taken (by James C. Bellows). We are grateful to the National Institute of Health for a grant with which the 2-m Jarrell-Ash spectrograph was purchased.

†Work supported under the Advanced Research Projects Agency Institutional Grant SD102, and the National Aeronautics and Space Administration Institutional Grant NGL 15-005-021.

[1]F. K. Fong, Phys. Rev. 187, 1099 (1969).
[2]R. H. Heist and F. K. Fong, Phys. Rev. B 1, 2970 (1970).
[3]F. K. Fong and E. Y. Wong, Phys. Rev. 162, 348 (1967).
[4]F. K. Fong, R. H. Heist, C. R. Chilver, J. C. Bellows, and R. L. Ford, J. Luminescence 2, 823 (1970).
[5]F. K. Fong, Phys. Rev. B 1, 4157 (1970).
[6]F. K. Fong and J. C. Bellows, Phys. Rev. B 1, 4240 (1970).
[7]F. K. Fong and J. C. Bellows, Phys. Rev. B 2, 2636 (1970).
[8]B. R. Judd, *Operator Techniques in Atomic Spectroscopy* (McGraw-Hill, New York, 1963), Chap. 2.
[9]W. E. Bron and W. R. Heller, Phys. Rev. 136, A1433 (1964).
[10]M. J. Weber, Phys. Rev. 171, 283 (1968).
[11]W. B. Gandrud and H. W. Moos, J. Chem. Phys. 49, 2170 (1968).
[12]L. A. Riseberg and H. W. Moos, Phys. Rev. 174, 429 (1968).
[13]L. G. Van Uitert, E. F. Dearborn, and W. H. Grodkiewicz, J. Chem. Phys. 49, 4400 (1968).
[14]F. K. Fong, J. A. Cape, and E. Y. Wong, Phys. Rev. 151, 299 (1966).
[15]R. Venkataraghavan, F. McLafferty, and J. Amy, Anal. Chem. 39, 178 (1967).
[16]G. D. Watkins, Phys. Rev. 113, 79 (1959); 113, 91 (1959).

PHYSICAL REVIEW B VOLUME 3, NUMBER 1 1 JANUARY 1971

Experimental and Theoretical Study of the Low-Lying Energy-Level Structure of Sm^{3+} in CaF_2†

H. Nara* and M. Schlesinger
Department of Physics, University of Windsor, Windsor 11, Ontario, Canada
(Received 3 August 1970)

The optical spectrum exhibited by the Sm^{3+} ion in CaF_2 is analyzed assuming both octahedral and trigonal site symmetries. Calculations were performed using a tensor operator technique in the complete intermediate-coupling scheme. The crystal field parameters and the root-mean-square (rms) deviations obtained are $B^{(4)}=-906$ cm^{-1} and $B^{(6)}=618$ cm^{-1}, with rms deviations of 48.1 cm^{-1} for the octahedral site symmetry; $B_0^{(2)}=118$ cm^{-1}, $B_0^{(4)}=-272$ cm^{-1}, $B_3^{(4)}=-296$ cm^{-1}, $B_0^{(6)}=38$ cm^{-1}, $B_4^{(6)}=-128$ cm^{-1}, and $B_6^{(6)}=1556$ cm^{-1}, with rms deviation of 35.4 cm^{-1} for the trigonal site symmetry. It is suggested that the sample on which the measurements were carried out contains Sm^{3+} ions occupying both octahedral and trigonal symmetry sites. It is also shown that crystal field theory with a single set of $B_q^{(k)}$ parameters is quite adequate to describe the energy levels lying below 11 000 cm^{-1}, above which a fairly large energy gap follows.

I. INTRODUCTION

The optical absorption, fluorescence, and paramagnetic resonance spectra of Sm^{3+} in CaF_2 have been investigated by several authors.[1–3] In particular, Rabbiner[2] investigated the florescence of Sm^{3+} in CaF_2 at tetragonal site symmetry and gave a theoretical interpretation.

The $CaF_2:Sm^{3+}$ system is of special interest as the strength of the crystal field is believed to be comparable to that of the spin-orbit interaction. This situation suggests that, in analyzing the experimental spectra, one should treat the system on the basis of the *complete* intermediate-coupling scheme. Fortunately, very accurate free-ion energy eigenvectors[4] are now available, and this treatment is possible in principle. This treatment, however, requires that very large matrices be diagonalized.

A fairly large energy gap of about 7500 cm^{-1} separates the lower-lying levels from higher ones. Crystal field matrix elements between the lower and upper groups of levels are small compared with the gap of 7500 cm^{-1}, and may be neglected. The lower group of levels may then be treated separately. Therefore one can work with matrices of considerably smaller dimensions, enabling one to perform the calculations of the type above.

Since the Sm^{3+} ion substitutes for Ca^{2+} ions in the CaF_2 crystal, there must be some kind of charge compensator so as to preserve charge neutrality. The actual site symmetry of the Sm^{3+} in the CaF_2 matrix will depend on the charge compensation mechanisms, which in turn depend on type and amount of impurities, growing conditions, thermal history, etc. Three main site symmetries[5] are possible for Sm^{3+} in CaF_2, namely, octahedral (O_h), tetrahedral (C_{4v}), and trigonal (C_{3v}) symmetries. Careful study of the influence of heat treatments[3] along with theoretical calculations enables one to classify the lines in the spectra according to their site symmetries. The heat treatment technique, however, is not practical for absorption lines lying below about 11 000 cm^{-1} because of opaque milkiness which is introduced in the crystals as a result of heat treatment. In this paper, where we are primarily concerned with the energy region up to 11 000 cm^{-1}, we shall at-